CONSTRAINT LOSS ESTIMATION SCHEMES IN DEEP AND SHALLOW THREE-DIMENSIONAL CRACK TIP FIELDS

LEONG KARH HENG

UNIVERSITI SAINS MALAYSIA

2017

CONSTRAINT LOSS ESTIMATION SCHEMES IN DEEP AND SHALLOW THREE-DIMENSIONAL CRACK TIP FIELDS

by

LEONG KARH HENG

Thesis submitted in fulfillment of the
requirements for the degree
of Master of Science

August 2017

ACKNOWLEDGEMENTS

This thesis is dedicated to everyone who embarks the journey of expanding the collection of knowledge and passion in carrying out this project.

First and foremost, highest gratitude is conveyed to Dr. Feizal Yusof, my project supervisor and thesis advisor, for seeing the promise of this thesis and achieving research conducted under his watchful eyes. His guidance and patience throughout the time are truly appreciated. Besides, his invaluable support and insightful suggestions in my numerical analysis, contributed tremendously to my project.

In addition, a sincere appreciation is delivered to Dr. -Ing Muhammad Razi Abdul Rahman for his continuous technical support on the High Performance Computing Cluster (HPC) in helping me to complete the project.

I would also like to thank the Ministry of Higher Education, Malaysia and the Institute of Postgraduate Studies, Universiti Sains Malaysia for providing me the financial support through MyBrain15 and Graduate Assistant Scheme grant respectively.

Last but not least, appreciations are dedicated to my coursemates and other friends for their inputs, supports and friendships. Not forgetting my lovely family, my deepest appreciation to them for their great patience and support over the years.

TABLE OF CONTENTS

LIST OF TABLES

LIST OF FIGURES

LIST OF ABBREVIATIONS

BLF	Boundary layer formulation
CCP	Center cracked tension panel
CT	Compact tension specimen
EPFM	Elastic-plastic fracture mechanics
EDI	Equivalent domain integral
HPC	High performance computing
HRR	Hutchinson, Rice & Rosengren
LEFM	Linear elastic fracture mechanics
LGC	Large geometry change
LSY	Large scale yielding
MBLF	Modified boundary layer formulation
SENB	Single edge notched bend bar
SENT	Single edge notched tension specimen
SSY	Small scale yielding
VCE	Virtual crack extension

LISTS OF SYMBOLS

a	Crack length
a_{eff}	Effective crack length
B	Physical specimen thickness
c	Uncracked ligament length
C_{ijkl} $(i, j, k, l$=1,2,3)	Stiffness tensor
E	Young's Modulus/Modulus of elasticity
$f_{ij}(i, j= r, \theta, z)$	Angular stress function in (r, θ, z) cylindrical coordinate system
$g_{ij}(i, j= r, \theta, z)$	Angular stress function for corner singularity fields
G	Shear modulus
$\mathcal{G}$	Energy released to propagate a crack
H	Specimen height
I (subscript)	Designation for mode I
$I(s)$	Interaction integral
I_n	Dimensionless function in HRR fields and $J - T_z$ fields
J	J-integral
J_{loc}	Local J-integral along a crack front
k	Yield stress in shear
K	Stress Intensity Factor
$\mathcal{K}$	Amplitude coefficient of stress dominant term
M	Global bending moment per unit thickness
n	Strain hardening exponent/rate
P	Applied load

P_0	Plastic limit load
r	Radial distance ahead of a crack tip
r_p	Plastic zone size
s	Order of stress singularity
S	Span between support of bend specimen
S_i (i=1,2,3)	Principal deviatoric stress components
t	Physical specimen thickness
T	T-stress
u_i (i=1,2,3)	Displacement components in (x_1, x_2, x_3) Cartesian coordinate system
v	Poisson's ratio
w	Strain energy density
W	Specimen width
W_s	Work required to create new crack surfaces
Y	Crack calibration factor
z	Distance measured from the free surface of a specimen
σ_{app}	Remotely applied stress
σ_{cr}	Critical stress for fracture to occur
σ_0	Yield strength/stress
$\sigma_{ij}(i, j$=1,2,3)	Stress components in (x_1, x_2, x_3) Cartesian coordinate system
$\sigma_{ij}(i, j = r, \theta, z)$	Stress components in (r, θ, z) cylindrical coordinate system
$\tilde{\sigma}_{ij}(i, j = r, \theta, z)$	Dimensionless stress functions for HRR fields and $J - T_z$ fields
σ_e, $\bar{\sigma}$	von Mises stress
σ_{kk}	Volumetric stress
σ_m	Mean stress

ε_{ij} $(i,j$=1,2,3)	Strain components in (x_1, x_2, x_3) Cartesian coordinate system
ε_0	Yield strain
α	Material constant
β	Stress biaxiality ratio
β^{thin}	Stress biaxiality ratio for thin specimen
β_c	Corner stress intensity factor
γ_s	Surface energy per unit area
γ_p	Plastic work done per unit area of crack surface area created
$\gamma_{T_z}, \gamma_\sigma$	Slope constants in the $J - \Delta\sigma$ approach
λ	Strength of corner singularity field
μ	Plastic deformation level
δ_{ij} $(i,j$=1,2)	Kronecker delta
Φ	Airy stress function
Π	Potential energy
Γ	Arbitrary contour around a crack tip

SKEMA ANGGARAN KEHILANAGN KEKANGAN DALAM MEDAN HUJUNG RETAKAN TIGA DIMENSI YANG DALAM DAN CETEK

ABSTRAK

Matlamat utama kajian ini adalah untuk memahami ciri-ciri kehilangan kekangan tiga dimensi dan melanjutkan pencirian skema anggaran kehilangan kekangan tiga dimensi seperti kaedah $J - T_z$ dan $J - \Delta\sigma$ dalam retakan. Skema anggaran kehilangan kekangan tiga dimensi dalam medan di hujung retakan elastik plastik telah disiasat dalam kajian ini dengan menggunakan bar retak bawah beban lenturan (SENB) dan plat retak tengah bawah beban tegangan (CCP). Model tersebut telah ditakrifkan dengan sifat bahan pengerasan terikan, $n = 3{,}6{,}13$ dan sifat bahan tanpa pengerasan ($n \to \infty$). Kehilangan kekangan dalam medan tegasan di hujung retakan didapati berubah dalam model dengan panjang retakan yang berlainan, $a/W = 0.1, 0.2, 0.3, 0.5$ and ketebalan yang berbeza, $B/(W - a) = 0.05, 1$.

Kehilangan kekangan di hujung retakan telah dikaji melalui pembandingan antara medan tegasan asimptotik bersifat tanpa pengerasan dengan penyelesaian hujung retakan terikan satah medan Prandtl dan penyelesaian hujung retakan tegasan satah Sham & Hancock. Kehilangan kekangan dalam satah didapati bertambah dengan tegasan T negatif apabila nisbah a/W dikecilkan. Penurunan ketebalan model juga didapati mengurangkan kehilanagan kekangan dalam satah kerana tegasan T meningkat dalam model yang nipis. Kehilangan kekangan luar satah diperhatikan di kawasan dari satah tengah ke permukaan bebas dalam semua model. Medan tegasan di permukaan bebas tidak dapat mencapai keadaan tegasan satah penuh kerana dipengaruhi oleh medan singulariti penjuru. Medan tegasan deviatorik adalah unik dalam semua model dan tidak bergantung pada kehilangan kekangan dalam satah dan

luar satah. Skema anggaran kehilangan kekangan juga dikemukakan untuk tegasan lingkar di depan retakan dengan menghubungkaitkan kehilanagan kekangan dengan magnitud tegasan T.

Keberkesanaan kaedah $J - T_z$ dan kaedah $J - \Delta\sigma$ dalam mencirikan medan di hujung retakan tiga dimensi juga dibincangkan. Pemerolehan terperinci dan algorithma untuk mengira kaedah $J - T_z$ telah ditunjukkan. Kaedah $J - T_z$ didapati bahawa gagal menggambarkan medan di hunjung retakan model yang menunjukkan kehilangan kekangan dalam satah. Kaedah $J - T_z - Q$ juga dikesahkan dengan mengunakan parameter Q terikan satah. Kaedah $J - T_z - Q$ didapati bahawa membuat anggaran berlebihan tentang kehilangan kekangan dalam satah dalam model nipis yang menunjukkan tegasan T negatif seperti model CCP nipis. Manakala, kaedah $J - \Delta\sigma$ adalah lebih bermanfaat kerana dapat menyifatkan kehilanagan kekangan dalam dan luar satah secara bersepadu dengan memplotkan tegasan paksi terhadap $J_{loc}/z\sigma_0$ parameter. Penggunaan kaedah $J - T_z$ memerlukan pertaburan T_z di depan retakan. Sebaliknya, aplikasi kaedah $J - \Delta\sigma$ adalah lebih mudah kerana kehilangan kekangan sepanjang retakan dapat dianggarkan melalui satu lengkungan unik untuk model yang mempunyai ketebalan yang berbeza.

CONSTRAINT LOSS ESTIMATION SCHEMES IN DEEP AND SHALLOW THREE-DIMENSIONAL CRACK TIP FIELDS

ABSTRACT

The primary goal of this study is to determine the three-dimensional constraint loss behavior and further extend the three-dimensional constraint loss estimation schemes of $J-T_z$ and $J-\Delta\sigma$ approaches in three-dimensional crack tip fields consisting of various crack configurations. The three-dimensional constraint loss estimation schemes in elastic-plastic crack tip fields were examined for a single edge notched bend bar (SENB) and a center cracked panel in tension (CCP). The finite element models were characterized with a strain hardening material, $n = 3, 6, 13$ and a non-hardening material, $n \to \infty$. The crack tip constraint loss was found to vary in the models with various crack length, $a/W = 0.1, 0.2, 0.3, 0.5$ and different thicknesses, $B/(W-a) = 0.05, 1$.

Crack tip constraint loss was studied by comparing the non-hardening crack tip asymptotic fields with the plane strain Prandtl's crack tip fields solutions and the plane stress Sham & Hancock's crack tip solutions. The in-plane constraint loss increased with a more negative T-stress following the reduction of a/W ratio. The thin model exhibited smaller the in-plane constraint loss as T-stress was less negative. The out-of-plane constraint loss occurred in all models at the region away from the midplane to the free surface. The radial and angular distribution of deviatoric stress field ahead of the crack tip was also found to be unique in all models and independent of the in-plane and the out-of-plane constraint loss. A constraint estimation loss scheme at $\theta = 0^\circ$ was proposed for the hoop stress along a crack front by correlating the constraint loss to the magnitude of the T-stress.

A detailed derivation and an algorithm to compute the $J - T_z$ approach were shown. The $J - T_z$ approach was unable to characterize the crack tip fields in the models that feature in-plane constraint loss and at the free surface due to a corner singularity field. The $J - T_z - Q$ approach using a plane strain Q parameter was evaluated. It was found that the $J - T_z - Q$ approach overestimated the in-plane constraint loss in a thin model with negative T-stress as seen in the thin CCP model. New equations were developed to extend the $J - \Delta\sigma$ approach in strain hardening models. The extended $J - \Delta\sigma$ approach offered a unified characterization of the in-plane and out-plane constraint loss along a crack front by plotting the normal stresses against a dimensionless $J_{loc}/z\sigma_0$ parameter. Unlike the $J - T_z$ approach that required an exact distribution of T_z along a crack front, the $J - \Delta\sigma$ approach is more advantageous as it can be applied immediately to approximate the constraint loss along a crack front by using a unified curve for the models with different thicknesses.

CHAPTER ONE
INTRODUCTION

1.1 Fracture Mechanics

Engineering structures can contain flaws and defects caused by manufacturing processes, inappropriate handling and material degradation. The flaws and defects can manifest into cracks. Structure with cracks will eventually become unstable and the cracks will propagate when the structures are loaded over a critical limit, eventually leading to a catastrophic failure at a load level lower than the designed limit.

Fracture mechanics is related to the study of failure mechanisms associated with cracks. Fracture toughness is proposed as the resistance of a material against the growth of crack. Fracture toughness is a material property which can be characterized by K in liner elastic materials or J parameter in elastic-plastic materials. To measure the fracture toughness, a standard procedure for the fracture toughness test is documented in the American Society for Testing and Materials (ASTM-E1820-11, 2011) and the British Standard Institution (BS-EN-ISO-12737, 2011). Standard test specimens such as single edge notched bend bar (SENB), center cracked tension panel (CCP) and compact tension (CT) specimens were usually employed in the fracture toughness test with a strict geometry requirement. A test specimen must be thick enough ($B/W \geq 0.5$) and possess a deep crack with a crack length of $0.45 \leq a/W \leq 0.5$. The strict geometry requirements were imposed to ensure to that the crack tip is fully constrained so that a lower bound fracture toughness value can be obtained from the test specimen.

1.2 Problem Statement

Problem arises in measuring the fracture toughness when the crack tip constraint is lost. For instance, the crack length in the interested geometry does not comply with the size requirements in the fracture toughness standard procedure. In engineering applications, the defects can be characterized as deep and shallow cracks. Specimens loaded in bending with crack length, $a/W < 0.3$ and specimens loaded in tension with crack length, $a/W < 0.5$ were categorized as shallow cracked specimens (Al-Ani & Hancock, 1991). Shallow cracks were commonly found in a welded joint, a heterogeneous region that involves two materials, and locations that are subjected to intense loading like cutting edges. Two dimensional analyses by (Al-Ani & Hancock, 1991; O'Dowd & Shih, 1991) showed that a shallow cracked specimen possessed a lower crack tip stress due to the in-plane crack tip constraint loss which resulted in a higher fracture toughness for the shallow cracked specimen. If the standard fracture toughness test is applied indiscriminately onto a shallow cracked structure, the fracture toughness will be overestimated. To alleviate this problem, two-parameter fracture mechanics approaches such as $K/J - T$ (Betegón & Hancock, 1991) and $J - Q$ (O'Dowd & Shih, 1991; O'Dowd & Shih, 1992) and $J - A_2$ (Chao et al, 1994; Yang et al, 1993a; b) were proposed to quantify the in-plane crack tip constraint loss.

The two-parameter approaches were designed for the evaluation of two-dimensional crack problems but the out-of-plane constraint effect was neglected. The crack tip constraint loss in a three-dimensional cracked body consists of the in-plane and out-of-plane constraint loss. The out-of-plane constraint loss was found to occur in the thickness direction from the midplane to the free surface of a specimen (Levy et al, 1971). New methodologies were suggested to describe the constraint loss in the three-dimensional crack tip fields such as the $J - T_z$ (Guo, 1993a), the $J - \Delta\sigma$ (Yusof,

2006), the $J - A_c$ (Mostafavi et al, 2009) and the $J - A_p$ (Yang et al, 2013) approaches. The $J - A_c$ and $J - A_p$ approaches characterized the in-plane and out-of-plane constraint losses in a unified curve by evaluating the plastic zone size and the area of equivalent plastic strain isoline ahead of a crack tip respectively. However, the $J - A_c$ and $J - A_p$ approaches were empirical as they require experimental testing and finite element analysis to construct a unified curve for the evaluation of fracture toughness for a given material. Moreover, the $J - A_c$ and $J - A_p$ only estimate fracture toughness but provide no insight on the state of local crack tip stress fields which is fundamental to the fracture mechanics framework for the assessments of fracture toughness.

In this study, the interest is focused on the $J - T_z$ and $J - \Delta\sigma$ approaches because they were based on the analysis of the state of crack tip stresses similar to the $J - Q$ approach. Current available literatures on the $J - T_z$ and $J - \Delta\sigma$ approaches were limited to specific crack geometries and material properties. Thus, the present research is motivated to extend the application of the approaches and to study the effectiveness of the $J - T_z$ and the $J - \Delta\sigma$ characterization for a wider range of crack configurations. The behavior of three-dimensional constraint loss will be firstly studied before extending the characterization of these three-dimensional approaches.

1.3 Objectives

The objectives of the present work are given as follows:

a) To determine the in-plane and the out-of-plane constraint losses in the non-hardening models under a tension and bending load for the deep and shallow cracks.

b) To quantify the deviation of the $J - T_z$ and $J - T_z - Q$ characterization from the crack tip fields in the strain hardening models under a tension and bending load for the deep and shallow cracks.

c) To measure the constraint loss along the crack front of models consisting of different thicknesses, strain hardening rates and crack lengths within a J-dominance limit through the $J - \Delta\sigma$ characterization.

1.4 Scope of Work

This study will focus on the understanding of the in-plane and the out-of-plane constraint loss behavior in a three-dimensional cracked geometry so that a generalized constraint estimation scheme can be developed. Detailed finite element analysis was conducted based on a highly constrained SENB model and an unconstrained CCP model in ABAQUS v6.12. The crack length and the thickness of the models were varied accordingly to demonstrate the in-plane and the out-of-plane crack tip constraint loss. In this context, the finite element models were designed with various crack lengths of $a/W = 0.5, 0.3, 0.2, 0.1$ and different thicknesses of $B/(W - a) = 1, 0.05$. The material properties of strain hardening exponents, $n = 3$, 6, 13 and ∞ were defined for the models.

The in-plane and the out-of-plane crack tip constraint loss behavior in a three-dimensional crack were studied by comparing the non-hardening crack tip stress fields to the analytical solutions such as the plane strain Prandtl field solutions (Rice, 1968b) and the plane stress (Sham & Hancock, 1999) solutions. Subsequently, the crack tip fields from the developed finite element models were validated against the $J - T_z$ approach (Guo, 1995) and the $J - \Delta\sigma$ approach (Yusof, 2006). The detailed derivation and the algorithm for computing the $J - T_z$ solutions were presented along with this work. The use of plane strain Q parameter with the $J - T_z$ approach to characterize the in-plane constraint loss was also discussed. The $J - \Delta\sigma$ approach (Yusof, 2006) were modified for the strain hardening models with deep and shallow cracks.

CHAPTER TWO
LITERATURE REVIEW

This chapter provides an overview on the development of fracture mechanics. The scope of the review covers the fundamental concepts in deformation, linear elastic fracture mechanics, elastic-plastic fracture mechanics, two-parameter fracture mechanics, characterization of three-dimensional elastic-plastic crack tip fields, corner singularity field and characterization of three-dimensional constraint loss.

2.1 Fundamentals of Deformation

This section covers the selected fundamental concepts used in the mechanics of materials, involving stress, strain, the associated material constitutive relations and plasticity.

2.1.1 Stress

The definitive text on elastic deformation can be found in (Timoshenko & Goodier, 1970). Stress is a fundamental concept in mechanics of materials. When a material is subjected to external load, internal forces will be produced as reaction forces to achieve a state of equilibrium. As these internal forces are distributed uniformly over an area of an imaginary internal surface, the intensity of the internal force is called stress. An arbitrary force in an orthogonal Cartesian coordinate system x_i $(i = 1, 2, 3)$ is applied onto a small cubic element as illustrated in Figure 2.1. Let the resultant force be a vector denoted as F_j due to the action across the area of cubic element, A_i. Then, the stress on the element can be expressed as:

$$\sigma_{ij} = \lim_{A_i \to 0} \frac{F_j}{A_i} \tag{2.1}$$

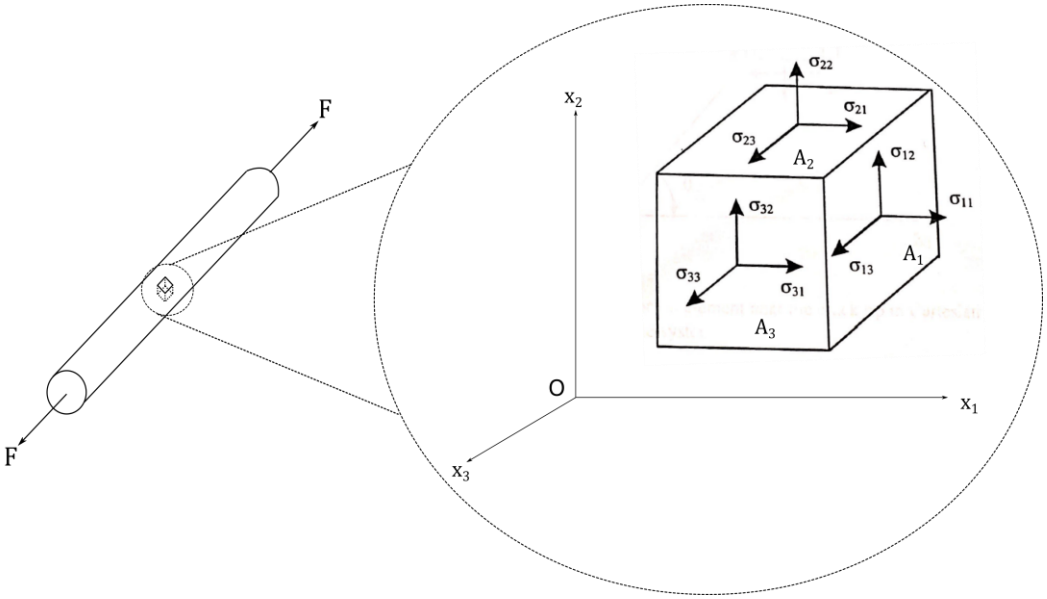

Figure 2.1: Stress components referred to Cartesian coordinates axes.

As seen from Figure 2.1, the stress components are presented as a second order tensor, σ_{ij} with $i, j = 1, 2, 3$. This means that in each axis, each stress component, σ_{ij} has its own magnitude that depends on the direction of axes, in which its first subscript, i indicates the direction of the normal to the plane under considerations while subscript j refers to the direction of force component. When $i = j$, σ_{ij} is acting perpendicular to the surface area, thus it is called as normal stress. For $i \neq j$, the stress component is acting in the plane and it is referred as the shear component of stresses. By considering that the cubic element is under equilibrium, the stress tensor σ_{ij} is essentially similar to σ_{ji}, implying that the symbols for the shear stress components can be reduced to three as follows:

$$\sigma_{12} = \sigma_{21}, \qquad \sigma_{23} = \sigma_{32}, \qquad \sigma_{13} = \sigma_{31} \tag{2.2}$$

For a body under static equilibrium, the stresses acting on a body must satisfy a set of differential equations known as the equilibrium equations, which in the absence of body force can be given as:

$$\frac{\partial \sigma_{11}}{\partial x_1} + \frac{\partial \sigma_{12}}{\partial x_2} + \frac{\partial \sigma_{31}}{\partial x_3} = 0 \quad (a)$$

$$\frac{\partial \sigma_{12}}{\partial x_1} + \frac{\partial \sigma_{22}}{\partial x_2} + \frac{\partial \sigma_{23}}{\partial x_3} = 0 \quad (b) \qquad (2.3)$$

$$\frac{\partial \sigma_{31}}{\partial x_1} + \frac{\partial \sigma_{23}}{\partial x_2} + \frac{\partial \sigma_{33}}{\partial x_3} = 0 \quad (c)$$

Within a body, there always exists three planes which are mutually perpendicular to each other with zero shear stress. The normal stresses acting on these planes are thus referred to as the principal stresses. The corresponding principal stresses are also known as the extremum value of normal stresses and are independent of the choice of the coordinate system. In a two-dimensional plane given in Mohr's Circle, the principal stresses can be presented as σ_1 and σ_2 as below:

$$\sigma_{1,2} = \frac{\sigma_{11} + \sigma_{22}}{2} \pm \sqrt{\left(\frac{\sigma_{11} - \sigma_{22}}{2}\right)^2 + {\sigma_{12}}^2} \qquad (2.4)$$

For a three-dimensional body, the principal stresses are denoted as σ_1, σ_2, σ_3 with a convention that $\sigma_1 \geq \sigma_2 \geq \sigma_3$.

All the prior stress components mentioned are in the form of a Cartesian coordinate system. Cartesian stresses can be transformed into the cylindrical state through stress transformation equations. The cylindrical coordinates system is usually preferred when dealing with a crack problem with cylindrical symmetry. The stresses in cylindrical coordinate system (Figure 2.2) can be expressed in terms of Cartesian stress components as:

$$\sigma_{rr} = \sigma_{11}cos^2\theta + \sigma_{22}sin^2\theta + 2\sigma_{12}sin\theta cos\theta \qquad (a)$$

$$\sigma_{\theta\theta} = \sigma_{11}sin^2\theta + \sigma_{22}cos^2\theta - 2\sigma_{12}sin\theta cos\theta \qquad (b) \qquad (2.5)$$

$$\sigma_{r\theta} = (\sigma_{22} - \sigma_{11})sin\theta cos\theta + \sigma_{12}(cos^2\theta - sin^2\theta) \; (c)$$

where σ_{rr} is the normal stress component in radial direction, $\sigma_{\theta\theta}$ is defined as the hoop stress in the circumferential direction and $\sigma_{r\theta}$ is the shear stress acting on a $r - \theta$ plane, where θ is the angle measured from the x_1 axis (usually taken as counter clockwise).

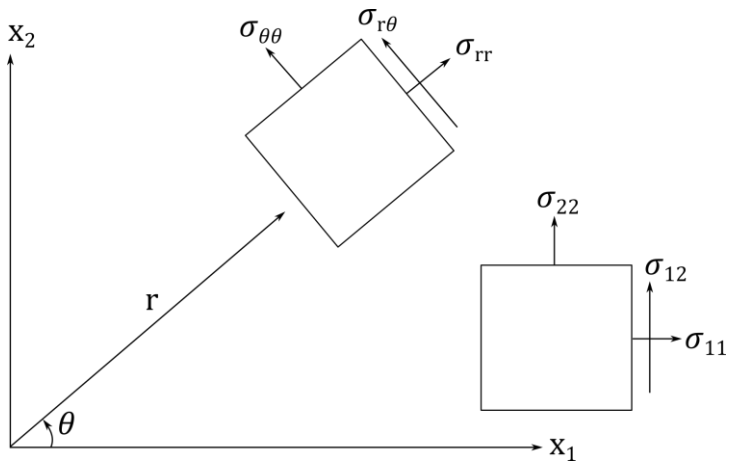

Figure 2.2: Stress components referred to cylindrical coordinates axes.

Similarly, to transform stress components from the cylindrical coordinate system into Cartesian form, a reverse transformation is given as:

$$\sigma_{11} = \sigma_{rr}cos^2\theta + \sigma_{\theta\theta}sin^2\theta - 2\sigma_{r\theta}sin\theta cos\theta \qquad (a)$$

$$\sigma_{22} = \sigma_{rr}sin^2\theta + \sigma_{\theta\theta}cos^2\theta + 2\sigma_{r\theta}sin\theta cos\theta \qquad (b) \qquad (2.6)$$

$$\sigma_{12} = (\sigma_{\theta\theta} - \sigma_{rr})sin\theta cos\theta + \sigma_{r\theta}(cos^2\theta - sin^2\theta) \; (c)$$

The stress tensor can also be expressed as the sum of the hydrostatic stress, σ_m and its deviatoric components, s_{ij}. Hydrostatic stress, σ_m is defined as the mean of the

three normal stresses, that its magnitude varies with the changes in body volume. It is therefore written as:

$$\sigma_m = \frac{1}{3}(\sigma_{11} + \sigma_{22} + \sigma_{33}) = \frac{\sigma_{kk}}{3} \tag{2.7}$$

where σ_{kk} is known as the volumetric stress which causes a body to change in volume. The deviatoric stress, s_{ij} is related to the shape change or distortion occurred on a body. The deviatoric stress is thus given as:

$$s_{ij} = \sigma_{ij} - \frac{\sigma_{kk}}{3}\delta_{ij} \tag{2.8}$$

where δ_{ij} is the Kronecker delta. If $i = j$, then $\delta_{ij} = 1$. Otherwise, when $i \neq j$, then $\delta_{ij} = 0$.

2.1.2 Strain

Under a multi-axial loading, the relative displacement of an infinitesimal element in a deformed body can be resolved into three components as u, v, w parallel to the x_1, x_2 and x_3 axes respectively. The displacement components can be measured in terms of a unit elongation or strain. Similar to stress, the strain components can be expressed in tensor notations as ε_{ij} which can be divided into normal strain components ($i = j$) and shear strain components ($i \neq j$). For normal strain components, they are expressed as:

$$\varepsilon_{11} = \frac{\partial u}{\partial x_1}, \qquad \varepsilon_{22} = \frac{\partial v}{\partial x_2}, \qquad \varepsilon_{33} = \frac{\partial w}{\partial x_3} \tag{2.9}$$

The shear strain components can be presented in the following form:

$$\varepsilon_{12} = \frac{1}{2}\left(\frac{\partial u}{\partial x_2} + \frac{\partial v}{\partial x_1}\right) \qquad (a) \tag{2.10}$$

$$\varepsilon_{23} = \frac{1}{2}\left(\frac{\partial v}{\partial x_3} + \frac{\partial w}{\partial x_2}\right) \qquad (b)$$

$$\varepsilon_{31} = \frac{1}{2}\left(\frac{\partial w}{\partial x_1} + \frac{\partial u}{\partial x_3}\right) \qquad (c)$$

All the strain components are not independent, but they are related to each other as they are in function of displacements. In a deformed body, the relationships between strain components are governed by a set of equations known as the strain compatibility equations. Compatibility equations provide conditions that must be satisfied by strains in all materials. The compatibility equations to be satisfied in a three-dimensional body are written as:

$$\begin{aligned}
&\frac{\partial^2 \varepsilon_{11}}{\partial {x_2}^2} + \frac{\partial^2 \varepsilon_{22}}{\partial {x_1}^2} = 2\frac{\partial^2 \varepsilon_{12}}{\partial x_1 x_2} && (a)\\
&\frac{\partial^2 \varepsilon_{22}}{\partial {x_3}^2} + \frac{\partial^2 \varepsilon_{33}}{\partial {x_2}^2} = 2\frac{\partial^2 \varepsilon_{23}}{\partial x_2 x_3} && (b)\\
&\frac{\partial^2 \varepsilon_{33}}{\partial {x_1}^2} + \frac{\partial^2 \varepsilon_{11}}{\partial {x_3}^2} = 2\frac{\partial^2 \varepsilon_{13}}{\partial x_1 x_3} && (c)\\
&\frac{\partial^2 \varepsilon_{11}}{\partial x_2 x_3} = \frac{\partial}{\partial x_1}\left(-\frac{\partial \varepsilon_{23}}{\partial x_1} + \frac{\partial \varepsilon_{13}}{\partial x_2} + \frac{\partial \varepsilon_{12}}{\partial x_3}\right) && (d)\\
&\frac{\partial^2 \varepsilon_{22}}{\partial x_1 x_3} = \frac{\partial}{\partial x_2}\left(\frac{\partial \varepsilon_{23}}{\partial x_1} - \frac{\partial \varepsilon_{13}}{\partial x_2} + \frac{\partial \varepsilon_{12}}{\partial x_3}\right) && (e)\\
&\frac{\partial^2 \varepsilon_{33}}{\partial x_1 x_2} = \frac{\partial}{\partial x_3}\left(\frac{\partial \varepsilon_{23}}{\partial x_1} + \frac{\partial \varepsilon_{13}}{\partial x_2} - \frac{\partial \varepsilon_{12}}{\partial x_3}\right) && (f)
\end{aligned} \qquad (2.11)$$

2.1.3 Elastic Constitutive Relation

Under linear elasticity, any deformation that occurs on a body is reversible as soon as the load is removed. In this case, the displacement of the body is proportional to the applied force, and this proportionality can be described in a basic relation called as the Hooke's Law. If the basic relation is extended into the three-dimensional cases

and applied over an infinitesimal area and length, a generalized Hooke's Law equation is obtained as follows:

$$\sigma_{ij} = C_{ijkl}\varepsilon_{kl} \tag{2.12}$$

where C_{ijkl} is a fourth order tensor known as the stiffness tensor with i, j and k, l =1, 2, 3. Since each subscript corresponds to three values, it would mean that the stiffness tensor has a total of $3^4 = 81$ independent elements.

From symmetric consideration, components of stiffness tensor can be further reduced. For example, the stress symmetry and strain symmetry allow the stiffness tensor to be written as $C_{ijkl} = C_{jikl} = C_{ijlk} = C_{jilk}$. From thermodynamic considerations, the position for two pairs of subscripts within a stiffness tensor can be switched such that $C_{ijkl} = C_{klij}$. Under this rule, the resulting stiffness tensor has 21 independent elastic constants. Such stiffness tensor can only be seen in a fully anisotropic material. For linear elastic isotropic material, the number of independent elastic elements in stiffness tensor can be further reduced down to 2.

In an elastic isotopic solid, the stress-strain relations under a multiaxial loading are given as:

$$\varepsilon_{11} = \frac{1}{E}[\sigma_{11} - v(\sigma_{22} + \sigma_{33})] \quad (a)$$

$$\varepsilon_{22} = \frac{1}{E}[\sigma_{22} - v(\sigma_{11} + \sigma_{33})] \quad (b) \tag{2.13}$$

$$\varepsilon_{33} = \frac{1}{E}[\sigma_{33} - v(\sigma_{11} + \sigma_{22})] \quad (c)$$

where E is the modulus of elasticity and v is the Poisson's ratio. The stress strain relation can also be written in terms of shear modulus, G where $E = 2G(1 + v)$ as:

$$\sigma_{ij} = 2G\left(\varepsilon_{ij} + \frac{v}{1 - 2v}\delta_{ij}\varepsilon_{kk}\right) \tag{2.14}$$

Alternative form of the elastic stress-strain constitutive law in terms of a stress deviator is also presented as follows:

$$\varepsilon_{ij}^{e} = \frac{1}{E}\left[(1+v)s_{ij} + \left(\frac{1-2v}{3}\right)\delta_{ij}\sigma_{kk}\right] \tag{2.15}$$

2.1.4 Plane States of Stress and Strain

Plane states of stress and strain are frequently used in engineering problems to simplify the problems without the need to consider a full three-dimensional case. With such feature, the two-dimensional idealisation concept ca-n be adopted in a finite element analysis to simplify a complex model.

Plane stress concept can be visualized by considering a thin plate loaded by force as shown in Figure 2.3. The thin plate has dimensions such that the dimensions in the x_1, x_2 direction are much greater than the dimension in the x_3 direction. The applied force is distributed uniformly across the boundary of the plate, so that there is no variation of the dimensions with respect to x_3. As a result, the stresses in x_3 direction have negligible order of magnitude and thus can be assumed as zero. Such state is defined as a generalized plane stress. The stress components in x_1 and x_2 direction can only vary slightly while the stress components in x_3 direction are:

$$\sigma_{33} = \sigma_{13} = \sigma_{23} = 0 \text{ and } \frac{\partial \sigma_{ij}}{\partial x_3} = 0 \quad (plane\ stress) \tag{2.16}$$

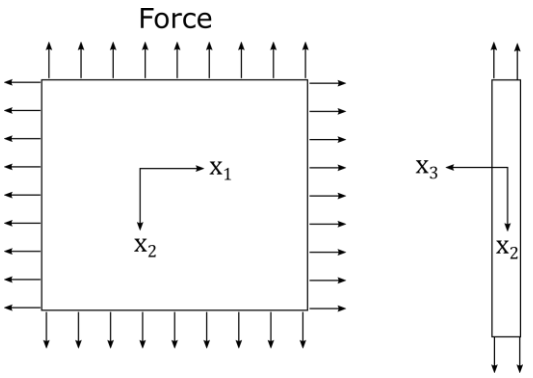

Figure 2.3: Plane stress condition in a stretched thin plate.

In a plane strain condition, a simplification approach is taken when the dimension of a body in the x_3 direction is very large compared to those in the x_1, x_2 directions. Consider a long prismatic body is loaded such that the two ends are fixed between two rigid smooth planes. The forces are applied uniformly across the surface of body and acting in perpendicular to the longitudinal axis of the body (refer to Figure 2.4). Also, the load is constant along the length in the x_3 direction. Thus, there is no displacement gradient that occurred along the length of the prismatic body because the deformation is restricted within the $x_1 - x_2$ plane. Under such conditions, a generalized plain strain state can be achieved with all strain components in the x_3 direction are restrained and become zero.

$$\varepsilon_{33} = \varepsilon_{13} = \varepsilon_{23} = 0 \ \ (plane\ strain) \tag{2.17}$$

By substituting $\varepsilon_{33} = 0$ into equation (2.13) (c), the stress in x_3 direction is written as:

$$\sigma_{33} = v(\sigma_{11} + \sigma_{22}) \tag{2.18}$$

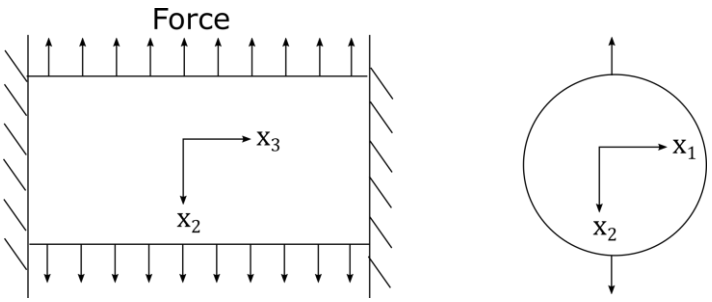

Figure 2.4: Plane strain condition in a loaded long prismatic body.

In a relatively thick solid block of material, when a load is applied, the plane state of stress and strain can coexist simultaneously. At the middle section of the material, as the material is constrained by the surrounding, the magnitude of ε_{33} is vanishingly small, thus a plane strain state prevails. The middle section of the block also possesses the highest value of σ_{33} but σ_{33} gradually decreases from the middle section to the free surface. In this context, the value of σ_{33} eventually becomes zero, leading to a plane stress state at the free surface.

2.1.5 Yield Criterion

The definitive text for plasticity is given in (Hill, 1998). Unlike linear elastic behaviour, plasticity is usually associated with irreversible deformation once a body is loaded beyond its yielding point. Yielding of an isotropic body is not affected by the hydrostatic pressure or applied tension, but it depends on the principal components of the deviatoric stress tensor (Hill, 1998). The principal components of the deviatoric stress, S_i can be expressed as functions of the stress invariants, J_2 and J_3 as below:

$$J_2 = \frac{1}{2}(S_1^2 + S_2^2 + S_3^2) = \frac{1}{2}s_{ij}s_{ij} \qquad (a)$$
$$J_3 = \frac{1}{3}(S_1^3 + S_2^3 + S_3^3) = \frac{1}{3}s_{ij}s_{jk}s_{ki} \quad (b) \qquad (2.19)$$

where S_i $(i = 1,2,3)$ is the principal component of deviatoric stress and s_{ij} is the deviatoric stress. It is useful to describe the stress state using stress invariants, J_2 and J_3 because their values are independent of coordinate systems selected.

The onset of plastic deformation can be described via two yielding criteria: Tresca yield criterion and von Mises yield criterion. For ductile materials, plasticity usually begins to develop as the crystal plane slips along the maximum shear stress surface. Therefore, the Tresca yield criterion states that yielding occurs when the maximum shear stress, τ_{max} exceeds the yield strength in shear, k.

$$\tau_{max} = k = \frac{\sigma_0}{2} = \text{Maximum of } \left|\frac{\sigma_1 - \sigma_2}{2}\right|, \left|\frac{\sigma_2 - \sigma_3}{2}\right|, \left|\frac{\sigma_3 - \sigma_1}{2}\right| \tag{2.20}$$

where σ_1, σ_2 and σ_3 are the principal stresses with $\sigma_1 \geq \sigma_2 \geq \sigma_3$. σ_0 is the yield stress. The Tresca criterion shows that the yield strength in shear is one half of the yield stress.

The von Mises criterion suggests that the yielding starts when the distortional energy stored in an isotropic material reaches a critical value which can be expressed as the equivalent stress, $\bar{\sigma}$.

$$\bar{\sigma} = \sqrt{\frac{1}{2}\left[\begin{matrix}(\sigma_{11} - \sigma_{22})^2 + (\sigma_{22} - \sigma_{33})^2 + (\sigma_{33} - \sigma_{11})^2 \\ +3{\sigma_{12}}^2 + 3{\sigma_{23}}^2 + 3{\sigma_{31}}^2\end{matrix}\right]} \tag{2.21}$$

Mathematically, von Mises criterion can also be related to J_2 stress invariant as follows:

$$\bar{\sigma} = \sqrt{3J_2} \tag{2.22}$$

By substituting equation (2.19) into (2.22), we can obtain

$$\bar{\sigma} = \sqrt{\frac{3}{2}s_{ij}s_{ij}} \tag{2.23}$$

Equation (2.23) shows a more compact form of equivalent stress in terms of the deviatoric stress. Also, when a ductile material is yielded under the von Mises

criterion, the J_2 stress invariant is equivalent to the square of the yield stress in shear, k^2 (Hill, 1998). Therefore, equation (2.22) will become:

$$\bar{\sigma} = \sigma_0 = \sqrt{3}k \tag{2.24}$$

2.1.6 Elastic-Plastic Constitutive Relation

In an isotropic body under uniaxial tension, the stress-strain relation varies linearly until the yielding commences as the stress level reaches the yielding stress, σ_0. This implies that the total strain, ε_{ij}^T during the deformation can be decomposed into the elastic and plastic strain tensor as shown below:

$$\varepsilon_{ij}^T = \varepsilon_{ij}^e + \varepsilon_{ij}^p \tag{2.25}$$

Equation (2.25) can also be rewritten in an incremental form as:

$$d\varepsilon_{ij}^T = d\varepsilon_{ij}^e + d\varepsilon_{ij}^p \tag{2.26}$$

Alternatively, equation (2.26) can be written compactly in terms of the deviatoric stress, s_{ij}:

$$d\varepsilon_{ij}^T = \frac{1}{E}\left[(1+v)s_{ij} - \left(\frac{1-2v}{3}\right)\delta_{ij}\sigma_{kk}\right] + \frac{3}{2}d\bar{\varepsilon}^p\frac{s_{ij}}{\bar{\sigma}} \tag{2.27}$$

where $d\bar{\varepsilon}^p$ is the equivalent plastic strain increment and $\bar{\sigma}$ is the equivalent stress. The first term represents the elastic incremental strain tensor and second term is the plastic strain increment. Equation (2.27) describes the incremental plasticity by relating the stresses to the strain increments, where the history of strain must be considered.

Under von Mises criterion, the equivalent plastic strain increment, $d\bar{\varepsilon}^p$ can be given as:

$$d\bar{\varepsilon}^p = \sqrt{\frac{2}{9}\begin{bmatrix}\left(d\varepsilon_{11}^p - d\varepsilon_{22}^p\right)^2 + \left(d\varepsilon_{22}^p - d\varepsilon_{33}^p\right)^2 + \left(d\varepsilon_{33}^p - d\varepsilon_{11}^p\right)^2 \\ + \frac{1}{3}\left({\gamma_{12}}^2 + {\gamma_{23}}^2 + {\gamma_{31}}^2\right)\end{bmatrix}} \quad (2.28)$$

and the equivalent plastic strain, $\bar{\varepsilon}_{ij}^p$ can be computed by integrating the equivalent plastic strain increment as:

$$\bar{\varepsilon}^p = \int d\bar{\varepsilon}^p \quad (2.29)$$

Contrary to the incremental plasticity, the concept of deformation plasticity is proposed to relate the total stress to the total strain. In this context, the deformation plasticity approximates the plastic behavior using the non-linear elasticity. The deformation plasticity will be violated if the plastic deformation history involves an unloading process. To describe the deformation plasticity, the elastic modulus, E in equation (2.13) can be replaced by the ratio of the equivalent stress to the equivalent strain, $\bar{\sigma}/\bar{\varepsilon}$ as:

$$\begin{aligned} \varepsilon_{11} &= \frac{\bar{\varepsilon}}{\bar{\sigma}}[\sigma_{11} - v(\sigma_{22} + \sigma_{33})] \quad (a) \\ \varepsilon_{22} &= \frac{\bar{\varepsilon}}{\bar{\sigma}}[\sigma_{22} - v(\sigma_{11} + \sigma_{33})] \quad (b) \\ \varepsilon_{33} &= \frac{\bar{\varepsilon}}{\bar{\sigma}}[\sigma_{33} - v(\sigma_{11} + \sigma_{22})] \quad (c) \end{aligned} \quad (2.30)$$

In the plastic region, the stress-strain relationship can be approximated in the form of a power law as:

$$\frac{\varepsilon_p}{\varepsilon_0} = \alpha\left(\frac{\sigma}{\sigma_0}\right)^n \quad (2.31)$$

where σ_0 is the reference stress normally taken as the yield stress and ε_0 is the reference strain. n is the strain hardening exponent and α is a proportionality constant that depends on the material. The strain hardening exponent ranges from 1 to ∞, in which $n = 1$ corresponds to a linear elastic material and $n = \infty$ represents a rigidly

plastic material. Under deformation plasticity, the overall stress-strain relationship in uniaxial tension can be described by the Ramberg-Osgood relation, that is written as:

$$\frac{\varepsilon}{\varepsilon_0} = \frac{\sigma}{\sigma_0} + \alpha \left(\frac{\sigma}{\sigma_0}\right)^n \tag{2.32}$$

These elastic-plastic constitutive relations are developed based on continuum approach, yet they are still relevant in the field of fracture mechanics. The small voids in a body grows, then coalescences to form a crack. When studying crack problems, the research interest usually focuses on the region surrounding the cracks, which is part of the considered continuum. The elastic-plastic constitutive relations are thus still valid in a cracked body, and they are fundamental to the theories of fracture mechanics as discussed in the following sections.

2.2 Linear Elastic Fracture Mechanics (LEFM)

Linear Elastic Fracture Mechanics (LEFM) refers to the field of fracture mechanics that applied specifically for linear elastic materials. LEFM evaluates the crack tip field using two methods: energy analysis and stress analysis. The energy analysis of LEFM centred on discussing the energy release rate, $\mathcal{G}$ and its relationship to K. In stress analysis of LEFM, the discussions are focused on the stress intensity factor, K which forms the core principle in LEFM.

2.2.1 Energy Based Approach

(Griffith, 1920) employed the first law of thermodynamics in explaining the crack advance based on a mica with a brittle behaviour. It was stated that the crack propagation will occur only if the potential energy of a solid is sufficient to meet the energy requirement for creating a new crack surface. The resistance to fracture in the

mica was assumed mainly due to the surface energy. When the potential energy released upon a crack growth is sufficient to overcome the surface energy developed, the crack extends. (Griffith, 1920) explained that there is always an equilibrium state attained between the potential energy and surface energy developed during the crack growth. The Griffith's energy balance per unit increment of crack extension is defined as:

$$\frac{dE}{da} = \frac{d\Pi}{da} + \frac{dW_s}{da} = 0 \tag{2.33}$$

where E is the total energy. Π is the potential energy and W_s represents the work required to create new crack surface.

Irwin continued working on Griffith' s energy balance by suggesting a more convenient form of the energetic approach for the crack advance in (Irwin, 1956). Based on the expression developed by (Inglis, 1913), Irwin expressed the potential energy, Π in terms of stress as

$$\Pi = \frac{\pi\sigma^2 a^2 t}{E'} \tag{2.34}$$

where E' is the Young' s modulus, with $E' = E$ for plane stress and $E' = \frac{E}{1-v^2}$ for plane strain with v as Poisson' s ratio. By substituting equation (2.34) into (2.33), the energy balance can be expressed as:

$$\begin{aligned} \frac{d\Pi}{da} &= \frac{dW_s}{da} \\ \frac{2\pi\sigma^2 at}{E'} &= 4at\gamma_s \end{aligned} \tag{2.35}$$

where γ_s is the surface energy per unit area. The critical stress for fracture to occur, σ_{cr} can thus be estimated as:

$$\sigma_{cr} = \sqrt{\frac{2\gamma_s E'}{\pi a}} \tag{2.36}$$

By taking Π as the potential energy in a plate of unit thickness, t, the amount of energy released to propagate a crack through unit distance da can be denoted as $\mathcal{G}$:

$$\mathcal{G} = \frac{d\Pi}{da} = \frac{\pi\sigma^2 a}{E'} \tag{2.37}$$

In this context, $\mathcal{G}$ is referred as the crack driving force which provides a quantitative measurement of force required to overcome the crack resistance for each increment of da.

The applicability of Griffith energy principle on engineering structure was also discussed in the work of (Orowan, 1954). He emphasized that Griffith energy principle can only be applied if the plastic deformation is either absent or confined to a very tiny region such that the global behaviour of structure is still considered as linear elastic. To account for the plastic flow, Orowan modified the expression in equation (2.36) for fracture stress as:

$$\sigma_{cr} = \sqrt{\frac{2(\gamma_s + \gamma_p)E'}{\pi a}} \tag{2.38}$$

where γ_p is the plastic work done per unit area of crack surface created.

In short, Griffith energy principle is a measure of global behaviour restricted to elastic response, but it provides little information on the local crack zone, such as the local crack tip stress field.

2.2.2 Stress Analysis of Cracks

An initial discourse on the crack tip stress analysis was given in (Inglis, 1913). In this context, Inglis developed a mathematical solution to quantify the stress field

around an elliptical hole in an elastic center cracked panel subjected to uniaxial tension. The stresses at the tip point of an elliptical hole, σ_{tip} with a major axis with a length of $2a$ and a minor axis with a length of $2b$ as shown in Figure 2.5 is expressed as:

$$\sigma_{tip} = \sigma_{app}\left(1 + \frac{2a}{b}\right) \tag{2.39}$$

where σ_{app} is the applied stress and can be normalized into $\sigma_{tip}/\sigma_{app}$ as a stress concentration factor. As the major axis, a grows and becomes larger relative to the minor axis, b, the curvature radius of the elliptical hole, ρ decreases and eventually takes the shape of a mathematically sharp crack. For this case, equation (2.39) becomes

$$\sigma_{tip} = \sigma\left(1 + 2\sqrt{\frac{a}{\rho}}\right) \tag{2.40}$$

where

$$\rho = \frac{b^2}{a} \tag{2.41}$$

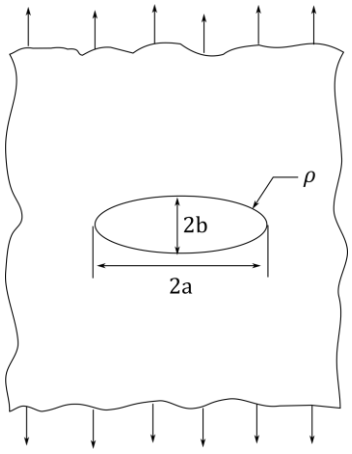

Figure 2.5: Elliptical hole in an infinite plate.

However, a paradox exists in Inglis' solution as his solution will predict an infinite stress at the tip of a mathematically sharp crack. This would mean any material

containing a sharp crack would fail instantly at the moment of the application of infinitesimal load, which is impossible in the real-life structure containing cracks. This limitation motivates the work of Griffith who considered to use energy approach to predict the crack advance instead of a local stress as discussed in the earlier section 2.2.1.

Later, the stress distribution analysis around the crack was further improved by by (Westergaard, 1939). The presented solutions described the normal stress and shearing stress of various two-dimensional crack problems. The Westergaard plane strain stress field for a center crack in an infinite plate under a biaxial loading was defined as:

$$\sigma_{11} = \frac{\sigma_{app}\sqrt{\pi a}}{\sqrt{2\pi r}} cos\frac{\theta}{2}\left(1 - sin\frac{\theta}{2}sin\frac{3\theta}{2}\right) \quad (a)$$

$$\sigma_{22} = \frac{\sigma_{app}\sqrt{\pi a}}{\sqrt{2\pi r}} cos\frac{\theta}{2}\left(1 + sin\frac{\theta}{2}sin\frac{3\theta}{2}\right) \quad (b) \qquad (r \ll a) \quad (2.42)$$

$$\sigma_{12} = \frac{\sigma_{app}\sqrt{\pi a}}{\sqrt{2\pi r}} sin\frac{\theta}{2}cos\frac{\theta}{2}cos\frac{3\theta}{2} \qquad (c)$$

where r represents the radial distance from crack tip, θ is the angle measured in the counter clockwise from the crack tip and a is the half crack length. The higher order terms are omitted from equation (2.42) as they become negligible compared to the leading terms as shown in the equation. The corresponding elastic stress fields to equation (2.42) are plotted in Figure 2.6.

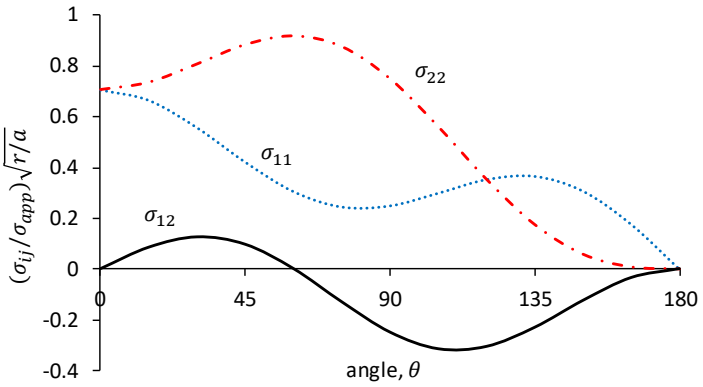

Figure 2.6: The plane strain Westergaard crack tip stress fields for a center cracked infinite plate under a biaxial loading.

2.2.3 Stress Intensity Factor, *K*

(Irwin, 1957) had generalized the Westergaard stress fields in equation (2.42) to be applicable to a wider range of cracked configurations by introducing a parameter denoted as K:

$$K = \sigma_{app}\sqrt{\pi a} \tag{2.43}$$

Equation (2.43 is derived based on the assumption that in a loaded linear elastic material, it must undergo proportional stressing where all the stress components increase in proportion to the remotely applied stress, σ_{app}. In this context, the crack tip stress can be related to σ_{app} by the parameter K and thus an alternative form of Westergaard stress fields can be written as:

$$\sigma_{ij}(r,\theta) = \frac{K}{\sqrt{2\pi r}} f_{ij}(\theta) \tag{2.44}$$

where $f_{ij}(\theta)$ is the angular stress function. In this context, $f_{ij}(\theta)$ depends on the loading mode (refer to Figure 2.7). Under mode I loading, $f_{ij}(\theta)$ is given as:

$$f_{rr(\theta)} = \frac{5}{4}\cos\left(\frac{\theta}{2}\right) - \frac{1}{4}\cos\left(\frac{3\theta}{2}\right) \quad (a) \tag{2.45}$$